https://doi.org/10.5194/egusphere-2025-365
Preprint. Discussion started: 10 February 2025

Learning Evaporative Fraction with Memory

Wenli Zhao[1, 2, 3], Alexander J. Winkler[1, 3], Markus Reichstein[1, 3], Rene Orth[1, 4], Pierre Gentine[2]

[1] Max Planck Institute for Biogeochemistry, Jena, Germany.
[2] Columbia University, New York, USA.
[3] ELLIS Jena Unit, Jena, Germany.
[4] Faculty of Environment and Natural Resources, University of Freiburg, Germany.

Correspondence to: Wenli Zhao (dr.wenli.zhao.pku@gmail.com)

Abstract. Evaporative Fraction (EF), the ratio of latent heat flux to the sum of sensible and latent heat flux, is a key metric of surface energy partitioning and water stress. Recognizing the importance of soil moisture and vegetation memory effect, we developed a machine learning (ML) model using Long Short-Term Memory (LSTM) unit, which include memory effects, to predict EF, based on eddy-covariance data from the combined ICOS, AmeriFlux, and FLUXNET2015 Tier 1 dataset across different plant functional types (PFT). The results show that the model can accurately capture and reconstruct the EF dynamics, particularly in the dry season and during drydowns, using routinely available weather observations, e.g., precipitation, net radiation, air temperature, vapor pressure deficit (VPD), and other static variables: PFT and soil properties. Specifically, there is a strong correlation (R^2 of 0.72) between the ensemble mean EF predictions and the observations on the test set, across sites spanning a large climate and ecosystem gradient. Second, we employ explainable ML techniques to elucidate the drivers of EF while accounting for the memory effect. Precipitation, VPD are two main drivers for woody savanna (WSA), savanna (SAV), open shrubland (OSH) and grassland (GRA) sites, while air temperature is dominate controlling factor in most forest sites, comprising deciduous broadleaf forest (DBF), evergreen needleleaf forest (ENF) and mixed forest (MF). Additionally, our findings reveal varying memory effects across different PFTs, as indicated by the contributions of antecedent time steps via integrated gradients. Specifically, GRA and WSA exhibited relatively lower memory effect contributions compared to forested sites. A detailed analysis of memory effects indicates their strong relationship with rooting depth, soil water holding capacity, and plant water use strategies, which collectively regulate the time scales of droughts. Notably, the learned memory effect across diverse PFTs could potentially serve as proxies for inferring vegetation rooting depth and assessing the plant water stress conditions. Our findings underscore the crucial influence of meteorological memory effect on EF predictions, particularly important for estimating future water stress, as the frequence and intensity of droughts are expected to rise.

1 Introduction

Evaporative Fraction (EF), which represents the fraction of available energy used for evapotranspiration, is defined as the ratio of latent heat flux (LE) to the sum of LE and sensible heat flux (H): $EF = \frac{LE}{LE+H}$ at the land surface. This ratio is

https://doi.org/10.5194/egusphere-2025-365
Preprint. Discussion started: 10 February 2025

critically linked to soil moisture availability, as it regulates evapotranspiration and therefore latent heat flux(Gentine et al., 2007; Nutini et al., 2014) and it also has a strong connection to vegetation greenness(Williams and Torn, 2015). Previous studies have shown that EF is mainly governed by root zone water availability and vegetation structure and is intrinsically linked to precipitation-supplied water resources(Bastiaanssen et al., 1997; Gentine et al., 2007; Ichii et al., 2009). As a result, EF can offer valuable insights into plant water status, and water stress, and their survival strategies during water stress conditions. A slowly declining EF during periods of droughts is indicative of a deep root system, which ensures sustained access to deep water stores(Dralle et al., 2020; Stocker et al., 2023) (Figure 1).

Accurate prediction of EF is essential for estimating evapotranspiration, monitoring plant water stress, and potentially inferring rooting depth(Collins and Bras, 2007; Fu et al., 2022; Liu et al., 2020; Wang et al., 2006). Among various environmental factors affecting EF, the soil moisture state dominates the day-to-day EF variations, particularly in water-limited regions(Dirmeyer et al., 2000; Dong et al., 2022; Haghighi et al., 2018; Lu et al., 2016). It serves as both a direct predictor of EF in prolonged dry spells and as a historical record, mirroring past climatic conditions and water availability — analogous to a memory effect. However, precise measurement or estimation of soil moisture in the rooting zone or plant water stress, is difficult or even impossible to acquire(O. and Orth, 2021; Skulovich and Gentine, 2023). This led to the development of various drought indices such as the Palmer Drought Severity Index, which try to infer the changes in soil moisture through a mechanistic, yet empirical, approach. These constraints underscore the importance of a more direct predictive model for EF, which could in turn be used as a more objective stress index, that can operate independently of soil moisture estimates and directly linked to surface evapotranspiration, emphasizing the incorporation of memory effects related to plant regulation within the algorithms(Kraft et al., 2019).

Advances in machine learning algorithms have shown promise in capturing complex hydrological processes, including surface fluxes, snowpack or streamflow prediction with the effect of lagged response(ElGhawi et al., 2023; Feng et al., 2020; Jiang et al., 2022; Pan et al., 2020; Reichstein et al., 2019, 2022; Zenone et al., 2022). However, few studies have directly incorporated the concept of memory effect in EF predictions. Yet, increasing evidence highlights the importance of memory effects in temporal prediction of water stress. Both soil moisture and EF dynamics rely not only on current precipitation status but also on historical precipitation patterns(Kraft et al., 2019; O. and Orth, 2021).

Long Short-Term Memory (LSTM) units have the ability to account for memory effects and can significantly enhance temporal prediction accuracy of non-linear processes(Fang and Shen, 2020; Jiang et al., 2020; Li et al., 2022). Thus, LSTM, a variant of recurrent neural networks, is particularly well suited for utilizing sequential data, an attribute suited for modeling EF dynamics. LSTM, with its recurrent cells, retains previous information from input sequences akin to how meteorological data, like precipitation, and its impact is retained over long periods of time as soil moisture or snowpack(Lees et al., 2021, 2022). This ability allows the model to reflect historical interactions between vegetation, atmospheric conditions, and water availability without relying on soil moisture as a direct input(Kraft et al., 2022; Lees et al., 2022). Instead, it infers such information through the memory effects captured within its recurrent cells. This enables the model to utilize both current and historical meteorological data, capturing the memory effect of meteorological data, e.g., past rainfall, to predict EF.

https://doi.org/10.5194/egusphere-2025-365
Preprint. Discussion started: 10 February 2025

In this study, we use a combination of networks of eddy-covariance data from ICOS, AmeriFlux, and FLUXNET2015 Tier 1 eddy-covariance (EC) dataset and remote sensing data to:

1) Develop an ML model, incorporating memory effects, to predict EF across diverse plant functional types (PFT).
2) Assess the model's predictive performance over various memory lengths.
3) Reconstruct EF dynamics during prolonged soil moisture dry-downs for unseen sites using the trained ML model.
4) Utilize integrated gradients methods, to explain the model and analyze the primary drivers of EF predictions across different plant functional types and further separate the feature contributions across time steps.
5) Investigate the relationship between memory effects across diverse PFTs and key factors such as rooting depths, soil water holding capacity (the soil matric suction) and aridity index, across different sites.

This methodology promises to illuminate plant water usage strategies especially during dry-downs through the lens of the memory effect, a perspective that becomes increasingly relevant as climate change escalates the frequency and severity of drought conditions.

https://doi.org/10.5194/egusphere-2025-365
Preprint. Discussion started: 10 February 2025

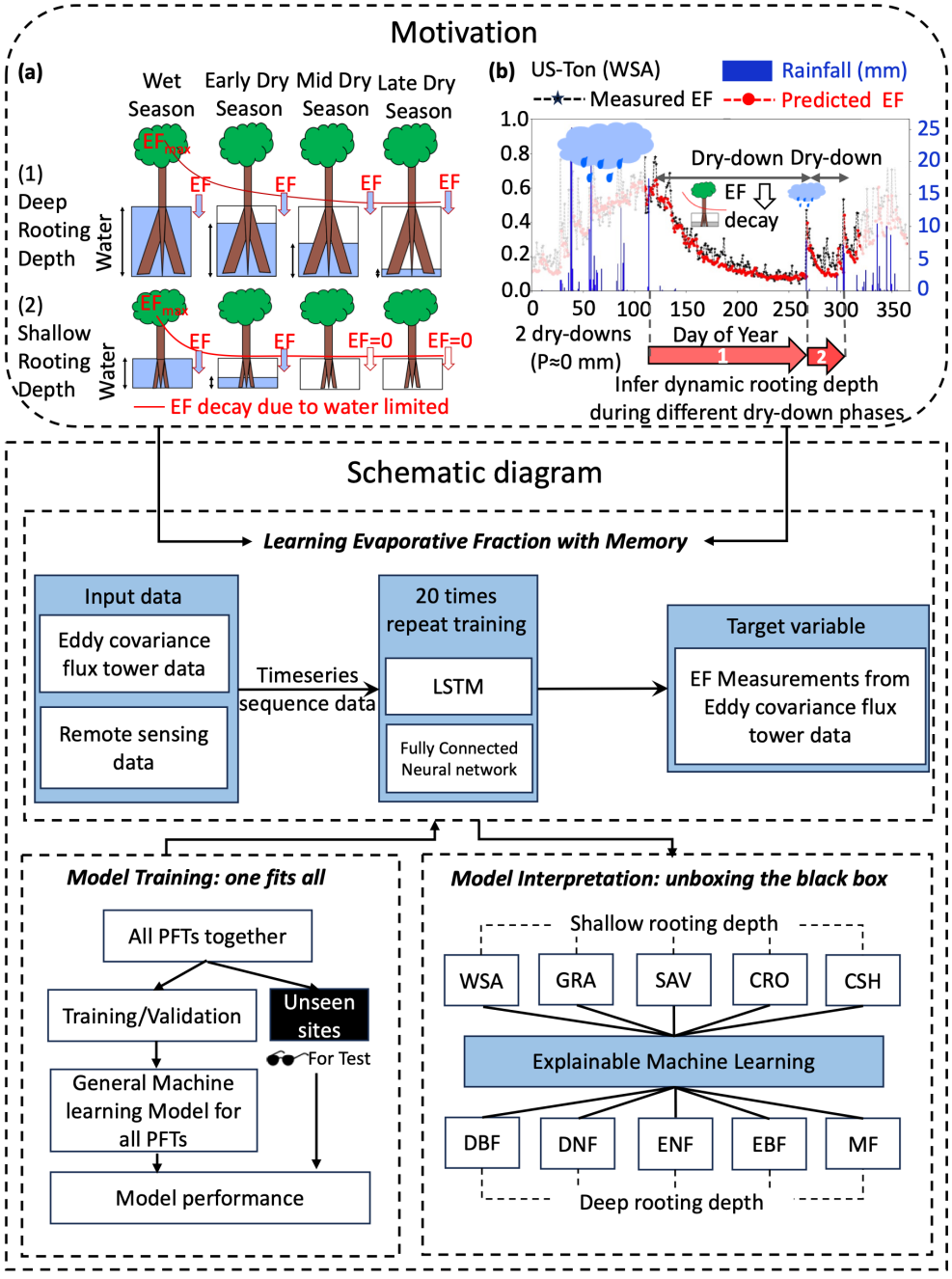

Figure 1. The motivation and schematic diagram of this study. Upper Panel: The motivation plot of this study. (a) indicates a water bucket model showing the EF decay during the dry downs. In the wet season, the precipitation fills up the vegetation water bucket and EF peaks. Then during the dry season, the vegetation will consume the available water storage during the wet season and thus EF decay could be observed. If the vegetation has a deep rooting depth, the EF decay will tend to be slow during the dry season. If the vegetation has a shallow rooting depth, the EF decay will tend to be fast during the dry season due to less available water storage compared to the deep rooting depth vegetation. Adapted from the Figure 3 in Ichii et al., 2009. (b) indicates a field experiment on a woody savanna site (US-Ton). The observations support our hypothesis in plot (a). Precipitation provides the available water storage and EF peaks, then there's a

https://doi.org/10.5194/egusphere-2025-365
Preprint. Discussion started: 10 February 2025

EF decay during the dry downs. The rooting depth information is hidden in the slow and fast EF dry downs. If we could predict EF accurately, we could potentially infer dynamic rooting depth and use EF as a direct water stress index. Lower Panel: The schematic diagram of this study. A long short-term model (LSTM) with memory effect is used here to capture the schemes expressed in the upper panel. A fully connected neural network is used here as a baseline. The model is trained using eddy covariance flux tower data and remote sensing data. We train a general model for all the sites and then use explainable machine learning technique to analyze the drivers for each plant functional types and sites. Further investigations have been conducted to explore the relationship between memory effects and rooting depth, soil water holding capacity and aridity index across various PFTs.

2 Data Collection and Preprocessing

2.1 Eddy covariance measurements

We used 215 eddy-covariance sites from the combined ICOS (https://doi.org/10.18160/2G60-ZHAK), AmeriFlux (https://ameriflux.lbl.gov/data/download-data/), FLUXNET 2015 tier 1 dataset (https://fluxnet.org/data/fluxnet2015-dataset/), covering 11 Plant Functional Types (PFTs) according to the IGBP (International Geosphere-Biosphere Programme) vegetation classification scheme(Loveland et al., 2000), including evergreen needleleaf forests (ENF), evergreen broadleaf forests (EBF), deciduous broadleaf forests (DBF), deciduous needleleaf forests (DNF), croplands (CRO), grasslands (GRA), savannas (SAV), woody savannas (WSA), closed shrublands (CSH), and mixed forests (MF), open shrub (OSH). The map of the site distributions is shown in Figure S1. Data for all the sites can be accessed via the links provided in Table S1. We first exclude the sites without latent heat flux, sensible heat flux, surface net radiation, precipitation, vapor pressure deficit (VPD), air temperature, wind speed measurements from the analysis; then we drop all cropland and wetland sites, as cropland sites are usually affected by management practices such as irrigation, and wetland sites usually have a perched water table. Next, we only kept the sites which has more than 10 years of observations after we applied the data preprocessing steps (further aggregated from half-hourly to daily scale), detailed in the following paragraph and supplementary materials (Text S1). These preprocessing steps help to reduce the data imbalance issue in parameter optimizations during the training of the models. The final dataset consists of 67 sites.

2.2 Evaporative Fraction Calculations

The Evaporative Fraction was calculated using the formula EF = LE/(H+LE), where LE represents the corrected latent heat flux and H the corrected sensible heat flux. We assume the errors in LE and H exhibit comparable magnitudes, as suggested by previous studies(Foken, 2008; Hollinger and Richardson, 2005; Richardson et al., 2006), and are uncorrelated. This assumption enables to mathematically eliminate the errors associated with the lack of energy balance closure(Schwalm et al., 2010).

https://doi.org/10.5194/egusphere-2025-365
Preprint. Discussion started: 10 February 2025

2.3 Leaf area index dataset

The leaf area index (LAI) data were obtained from the simultaneous MODIS product MCD15A3H using the Global Subset Tool (https://modis.ornl.gov/globalsubset/). The temporal resolution is 4 days. LAI does not significantly change within 4 days, so we used this LAI value as the daily input of our algorithms.

2.4 Soil attribute data

The soil attribute data is from SoilGrid with a resolution of 250 meters, including clay, silt and sand content(Poggio et al., 2021).

3 Methodology

3.1 Long Short-Term Memory Model

A machine learning model using the Long Short-Term Memory architecture, which explicitly accounts for memory effects, is used to predict the daily scale EF. We test different combinations of hyperparameters, including the number of LSTM layers and neurons per layer, to determine the most appropriate model structure (Figure S2). The finalized model structure consists of 3 layers with activation functions as follows: one LSTM layer with 128 neurons, fully connected dense layer with 36 neurons and one output dense layer with 1 neuron.

We choose dynamic variables including daily sum precipitation (P), daily mean wind speed (WS), daily mean surface net radiation (Rn), daily mean air temperature (Ta), daily mean VPD, LAI and site-specific static variables including soil properties and PFTs as the input features. In addition, annual mean P, annual mean Rn, annual mean Ta are also input of the model to account for climatic differences.

3.2 Fully connected Neural Network (NN) Model

To compare the role of memory effect captured by the LSTM model, we choose a fully connected neural network as a baseline for EF prediction. Like the process of defining the LSTM model structure, we tested different combinations of hyperparameters, including the number of fully connected layers and neurons per layer, while ensuring a fair comparison with the LSTM model. The final fully connected neural network model structure is as follows: it consists of two fully connected dense layer with 128 neurons, one fully connected dense layer with 36 neurons and one output dense layer with 1 neuron (Figure S2). The length of time series sequence data is same with the input for the LSTM model.

3.3 Training/Validation/Test Set Setups

The datasets are separated by site, with one site from each PFT randomly selected for testing and validation, and the remaining sites used for training. This ensures robust generalization and suitability for potential application for global

https://doi.org/10.5194/egusphere-2025-365
Preprint. Discussion started: 10 February 2025

upscaling efforts based on the climate reanalysis data. It is worth noting that we also experimented with a temporal split, which yields better model performance (achieving an R^2 of 0.80, as shown in Figure S3). However, considering future global upscaling, we opted for a site-based split here to ensure generalization.

Then we set up 20 models only varying in the initialization of the weights and biases of LSTM and NN and train each model with different memory lengths to reduce the randomness and obtain a measure of uncertainty. The memory length varies from 10 to 360 days with 10-day intervals (365 days is also added to test) to identify the most appropriate memory length that yields the best prediction skill (Figure 1). Early stopping is used to avoid overfitting and find the best model for prediction.

After 20 times' repeat training for each memory length, we also calculate the ensemble mean predictions (average value of the 20 models' predictions) as the robust EF prediction.

3.3 Model Interpretations – Integrated Gradients (IG)

Considering the potential collinearities among the predictors and the aim to attribute contributions to each time step, we implemented the integrated gradients techniques to further exploit the feature importance at each time step, revealing the specific contributions of inputs to daily EF predictions (see details in Text S2). Compared to permutation feature importance, this approach enables our temporal model to break down the overall importance of features into specific contributions at each time step(Molnar, 2019). This detailed analysis allows us to examine the response of plants across varying memory effects under extreme events or environmental conditions – a capability not present in non-temporal models.

4 Results and Discussions

4.1 Model Performance Across All Plant Functional Types

Figure 2 presents the efficacy of our trained LSTM models, in which we vary the memory length from 10 to 360 days (in 10-day intervals, with 365 days setting also tested). This variation reflects the extent of past temporal context considered in making the EF prediction for the current day. For each specific memory length, we repeated the training process for 20 times while sampling different initial parameters of the ML models. This approach mitigates the randomness inherent in the ML model parameter optimization and provides a quantification of uncertainty. The whole datasets were separated by site, with one site from each PFT randomly selected for testing and validation, and the remaining sites used for training (Methods). The results suggest that overall, the LSTM models achieved good accuracy in EF prediction, compared to the EF observations of EC towers for all test sites (at sites never seen by the model during the training and validation process). The model's predictive accuracy, as reflected by the mean R^2 values (mean R^2 of the 20 repeated models for each memory length), generally improved with longer memory lengths, stabilizing between 300 days and 365 days with R^2 values of 0.67, 0.68, 0.68, 0.68, 0.68, 0.67, 0.67 and 0.68, respectively, for memory windows ranging from 300 to 365 days. We also note that the ensemble mean of EF predictions from the 20 repeated models shows a higher R^2 compared to any individual model,

https://doi.org/10.5194/egusphere-2025-365
Preprint. Discussion started: 10 February 2025

achieving an R^2 of 0.72 for a memory length of 365 days (dashed line in Figure 2(a)), when compared to the observations at
175 EC sites. We thus suggest using an ensemble method for the final prediction.

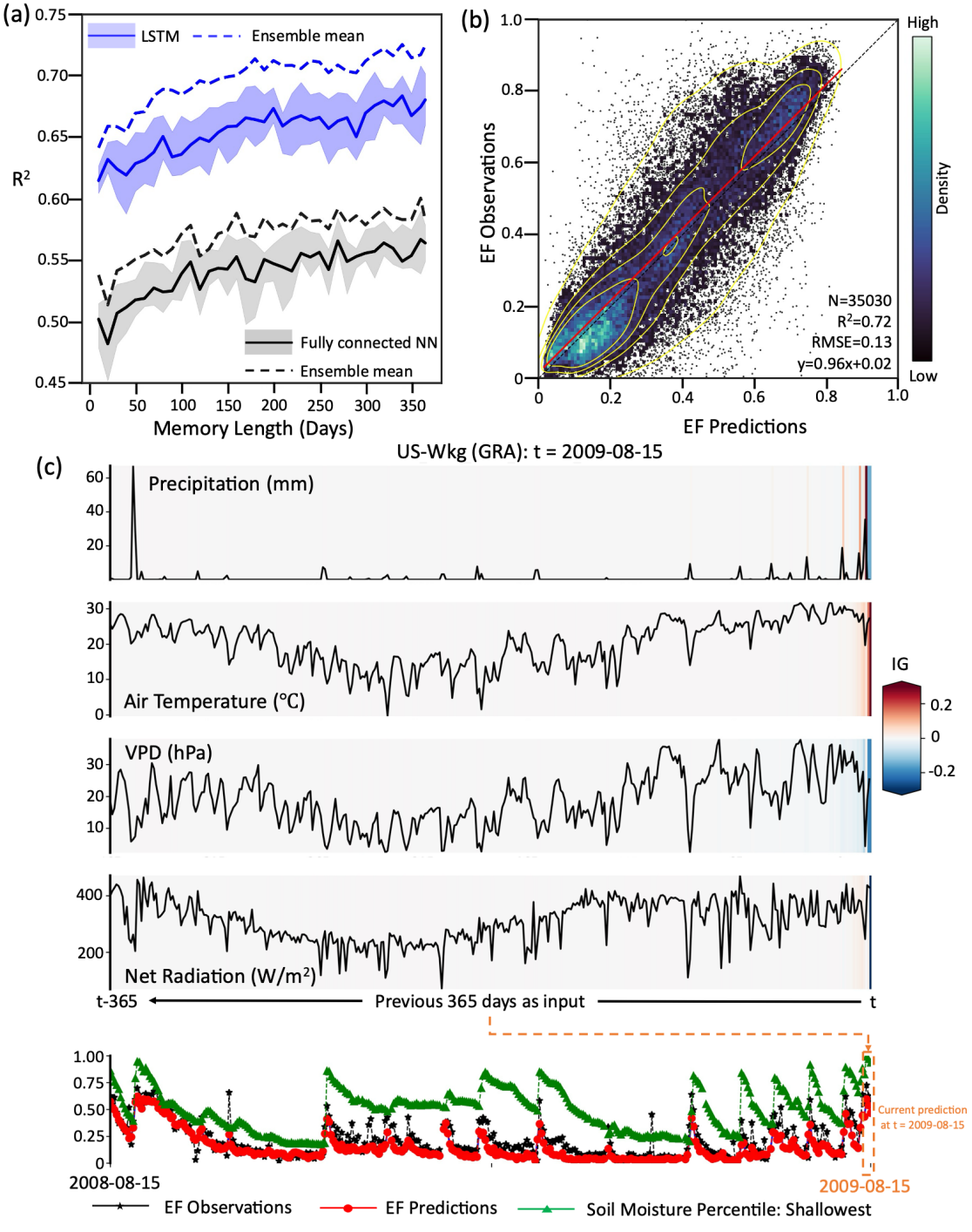

https://doi.org/10.5194/egusphere-2025-365
Preprint. Discussion started: 10 February 2025

Figure 2. Model performance across the sites in the test set. a) indicates the model performance for different memory length settings. The solid line indicates the mean R^2 of 20 repeated training models in the test set, while the shading bounds the interval of the 25th to 75th percentiles. The dashed line indicates the R^2 of ensemble EF predictions of 20 models with the EF observations. The x-axis denotes the memory length, reflecting the number of days of input time series sequence data utilized in model training. The memory length is from 10 to 360 days (with 10-day intervals, 365 days are also tested here). b) indicates the model performance with 365 days' time series data as input. The EF predictions shown here are based on the ensemble mean EF predictions of 20 repeated models. The density of scatter points is represented using shading colors. The diagonal black dashed line depicts the 1:1 line and the red solid line depicts the linear regression line. Note that N, R^2, and RMSE represent the number of points, coefficient of determination, and root mean square error, respectively. All the metrics are calculated using the test set data. c) indicates an example for the memory effect highlighted by the integrated gradients using the example of a grassland site (US-Wkg, 2009-08-15). The time series sequence data of the previous 365 days (2008-08-15 to 2009-08-15) are used to make the EF prediction at 2009-08-15. The integrated gradients highlight the impact of precipitation, air temperature, VPD, net radiation of previous time steps to the current EF predictions. Note that the integrated gradients for all the sites are summarized in the Figure 4, Figure 5, Figure 6 below.

In contrast, an instantaneous (i.e. without memory) fully connected neural network model, despite utilizing the same lengths of time series data, did not perform as well as the LSTM for EF prediction (Figure 2). This underscores the importance of the memory effect and the superiority of the LSTM architecture in accurately predicting EF. The LSTM model, comprising input, forget, and output gates, manages to long-range retain or discard patterns in meteorological data, thereby capturing long-term dependencies effectively. Crucially, this mechanism is analogous to a water infiltration and retention in the soil and slow evapotranspiration processes, where prior rainfall is conserved as soil moisture and later accessed by plants' root systems for plant function and growth(Dralle et al., 2020). Consequently, our model can accurately simulate the physical process of plant water usage during dry spells and its time dependence as sketched in Figure 1. The contribution of each individual time step indicated by the Integrated Gradients (see Methods) clearly shows the impact of previous rainfall on the current EF predictions (Figure 2(c)). This reflects the positive impact of previous precipitation (lag effect), especially closest to the prediction time, and negative impact of dry spells to EF predictions, exemplified by the 2009-08-15 data from the US-Wkg grassland site (Figure 2(c)). We summarize all the explainable IGs for all the sites in Figure 4, Figure 5 and Figure 6 (Section 3).

Nevertheless, we observed a consistent bias in the model's predictions at higher EF values for some sites, compared to lower ones, as depicted in Figure 2(b). A closer examination reveals that higher EF values typically occur at forested sites (ENF, EBF, DBF, DNF, MF), while lower EF values are found at non-forested sites (GRA, SAV, WSA, CSH, OSH). This prediction bias may be partially due to canopy interception effects, increasing rapidly EF at site, but also at times when eddy-covariance measurements are less reliable because of high relative humidity and dew, thus impacting the accuracy of EF observations(Lian et al., 2022). For example, a clear perturbation is observed in the EF observations at US-Moz (DBF) and CA-Qfo (ENF) site (Figure 3 (g) and (h)). Further investigation to enhance the model's predictive performance at these locations could yield to improvements and is left for future work, as it will have to be done in tandem with specific inspection of measurement biases. Instead, our focus in this manuscript is on drydowns.

https://doi.org/10.5194/egusphere-2025-365
Preprint. Discussion started: 10 February 2025

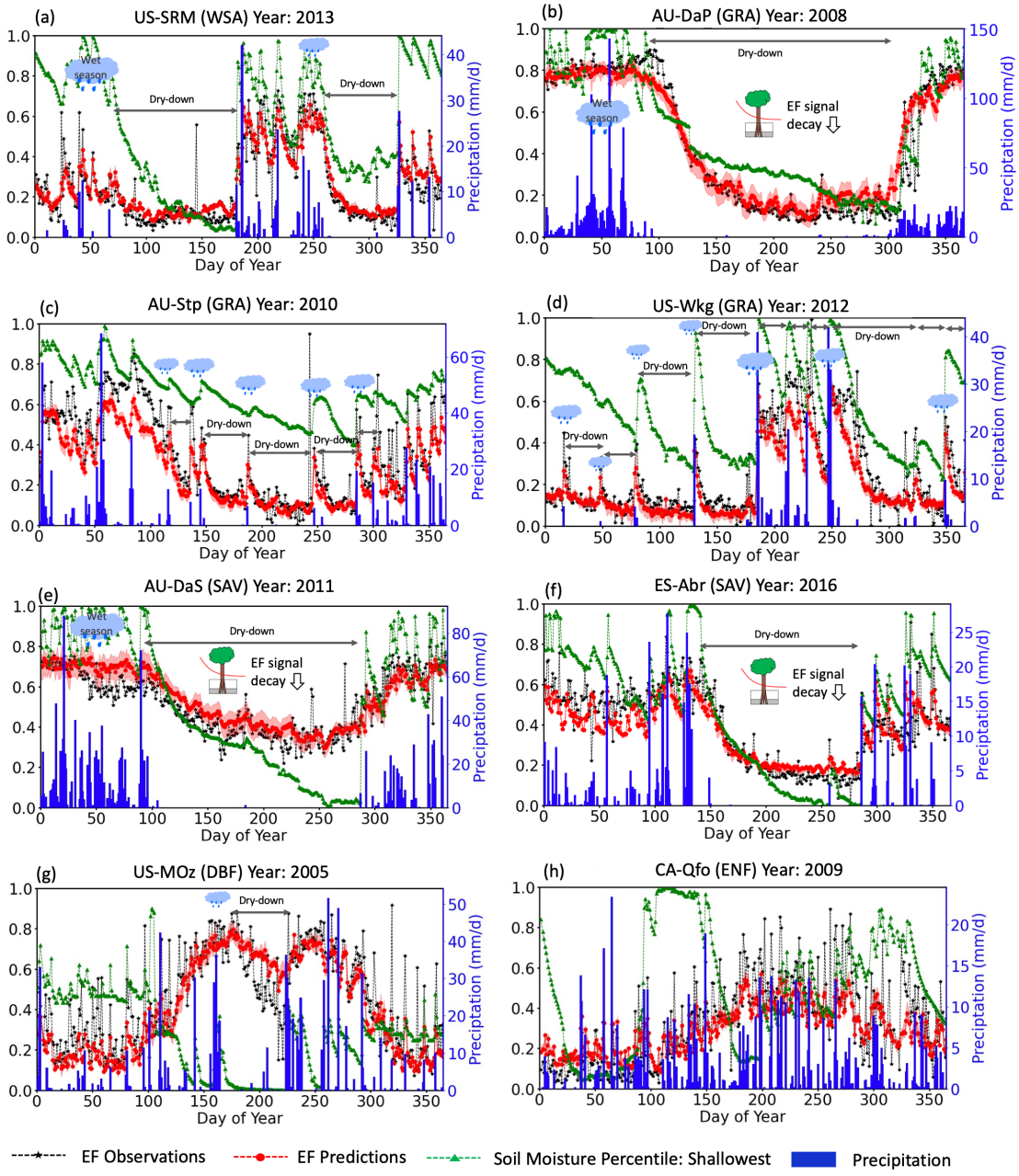

Figure 3. Prediction of Evaporative Fraction Dynamics for Unseen Sites Across Various Plant Functional Types. Daily time series of Evaporative Fraction (EF) dynamics for several cases of dry-down periods, as estimated by machine learning models considering memory effects. Blue bars show the observed daily sum precipitation (P), black curves show EF observations, red curves show EF predictions, green curves show soil moisture percentiles of the shallowest soil depth. The x-axis represents the day of year (DOY) of the whole year. Labels in the panels show the auxiliary information of the detected dry-down periods (GRA: grassland, WSA: woody savanna, SAV: savanna, DBF: deciduous broadleaf forest, ENF: evergreen needleleaf forest). The daily volumetric water content values are converted into percentiles, indicating the fraction of daily values lower than a specific value. Thus, the 100th percentile (or a percentile value of 1) represents the wettest soil conditions observed at a specific site throughout the study period, and the 0 percentile signifies the driest soil conditions. The length of time sequence input is set as 365 days for the machine learning model. The EF predictions here are

https://doi.org/10.5194/egusphere-2025-365
Preprint. Discussion started: 10 February 2025

using the ensemble mean EF predictions of 20 models with different initializations. Shaded areas represent regions of predictions uncertainty in the 25%-75% quartiles of these 20 repeat training models. Note all the results shown here are from the test set.

4.2 Reconstruction of Evaporative Fraction Dynamics During Soil Moisture Dry-Down Periods

Our model adeptly captures the observed EF dynamics as observed in the unseen sites, particularly during soil moisture dry-down periods across grassland, savanna and woody savanna sites, as illustrated in Figure 3. The decay in EF predictions aligns with the observed decline in shallow soil moisture, corroborating soil water processes where wet season precipitation supplies the initial water for prolonged dry periods which is then slowly decaying through evapotranspiration (only shallow soil moisture observations are used here for comparisons due to the data limitation). Consequently, EF peaks, and then gradually decreases at varying rates during drydown intervals, with a pace reflecting diverse evaporative demand and vegetation rooting depths and plant water usage strategies. For example, grasslands, with typically shallow roots, exhibit a faster EF decay compared to savannas, which suggest a deeper rooting system and/or lower canopy conductance for the latter (Figure 3(c), Figure 3(d), Figure 3(e), Figure 3(f)), consistent with in-situ observations(Dralle et al., 2020; Fan et al., 2017; Ichii et al., 2009; Seyfried and Wilcox, 2006). However, we also note the diversity of climatic environments in which the different grassland sites are situated. For instance, AU-DaP experiences sufficient precipitation only in certain seasons, whereas precipitation at AU-Stp is more evenly distributed throughout the entire year (Figure 3). Some grassland sites receive sufficient rainfall during the whole years like the deciduous broadleaf and evergreen broadleaf forest sites (see Figure S4). This leads to differences in the characteristics of their EF drydowns. The investigations of the variations in EF decay rates offers a promising avenue for inferring rooting depths, and plant water-use strategies across sites and underscores EF's potential as an indicator of vegetation-regulated water stress responses.

In contrast to the sporadic rainfall observed in grasslands and savannas, deciduous broadleaf forest and evergreen broadleaf forest sites experience abundant precipitation year-round. This abundance leads to significant fluctuations in EF observations, likely influenced by canopy interception, as discussed in the previous section. Overall, our time series analysis indicates the model's high predictive accuracy during plant water stress periods, showcasing superior performance for grasslands and woody savannas compared to the forests sites, which has fewer dry-down periods. The varied rates of dry-down likely reflect different plant rooting depths and water usage strategies, influencing drought time scales. This suggests that an optimal memory length for EF prediction may exist for each plant functional types or site.

4.3 Memory Effects: Uncovering Hidden Mechanisms in Plant Water Use Strategies

Delving into the causes of rapid and gradual EF decreases, we analyze the trained EF model using explainable machine learning techniques, namely integrated gradients (Molnar, 2019; Sundararajan et al., 2017). IG is a method for attributing the prediction of a neural network to its input features by integrating gradients along the path from a baseline input to the actual input. This analysis not only revealed the controlling factors in predicting EF but also delineated the temporal influences, allowing us to ascertain the general feature importance alongside the distinct contributions to each individual time step.

https://doi.org/10.5194/egusphere-2025-365
Preprint. Discussion started: 10 February 2025

Consequently, the feature importance obtained through IGs inherently includes the memory contributions from historical periods for each variable, thus potentially considering the memory effect and the legacy effect.

First, we summarize the IGs by calculating the relative contribution for each variable (in %). This is achieved by dividing the total sum of absolute IGs for each variable. For all the sites put together, the absolute IGs identified air temperature (25%) and precipitation (21%) as the most two influential drivers. This is followed by vapor pressure deficit (18%), PFT (17%), net radiation (8%), leaf area index (6%), and wind speed (5%). Precipitation feeds the available water resources, i.e., root-zone soil layer, used to sustain the ecosystem during droughts. The reason net radiation, which dictates energy input and drives evaporative demand leading to soil moisture and EF declines, may not appear as important in this analysis could be due to the consideration of memory or legacy effects by the temporal model. While net radiation might be crucial for the immediate impact on EF, when taking memory effects into account, other factors such as air temperature and precipitation become more dominant. This highlights the key role of memory effect when predicting EF and other land-atmosphere flux components. VPD provides a measure of atmospheric aridity, significantly affecting ET and thus EF. Interestingly, PFT has a reduced impact compared to climatic factors, as evidenced by the model's robust performance for completely unseen sites (Figure 2 and Figure 3). This suggests the model's potential for upscaling from local to global scales and thus its capacity to be used a stress index. LAI did not emerge as a dominant feature for EF prediction, partly due to spatial and temporal discrepancies in the MODIS LAI product (250 meters, 4-day) but also to the fact that most variability in EF at dry sites is due to soil moisture decay and driven by (lack of) precipitation. Cloud cover or aerosols may also contaminate the MODIS LAI data(Yang et al., 2006). Wind speed's minimal effect on EF predictions aligns with recent data-driven research(Gentine et al., 2011; Lhomme and Elguero, 1999; Zhao et al., 2019), showing that evapotranspiration is not strongly affected by wind speed. However, we also note that the significance of input features importance varies among different sites, different PFTs and climatic regions (Figure 4). In general, the water controls, i.e., precipitation, VPD are the two main drivers for most of woody savanna, savanna, open shrubland and grassland sites, while air temperature are dominate controlling factor for most of the forest sites for deciduous broadleaf forest, evergreen needleleaf forest and mixed forest sites, which is consistent with previous studies(Chen et al., 2018; Guérin et al., 2020).

https://doi.org/10.5194/egusphere-2025-365
Preprint. Discussion started: 10 February 2025

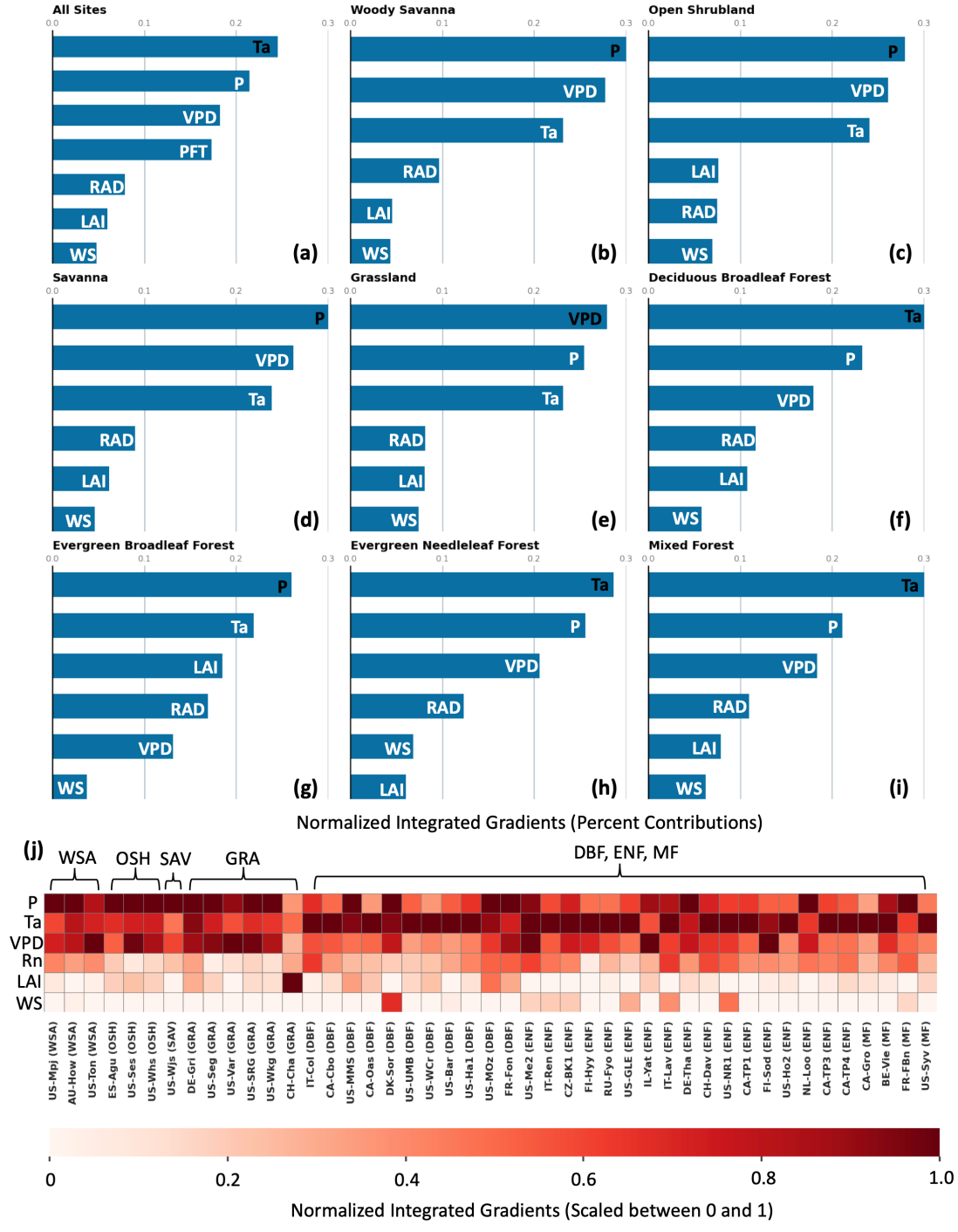

Figure 4. Feature Importance Revealed by the Temporal Evaporative Fractions Model Considering the Memory Effect. a indicates the overall feature importance across all the plant functional types. b, c, d, e, f, g, h, i represents the feature importance for woody savanna (WSA), open shrubland (OSH), savanna grassland (SAV), deciduous broadleaf forest (DBF), evergreen broadleaf forest (EBF), evergreen needleleaf forest (ENF), mixed forest (MF). Note that the IG values are normalized by percent contributions, that is, divided by the total sum of absolute IGs for all the variables shown here in each plot. Thus the values here indicate a relative percent contributions (e.g., 0.3

https://doi.org/10.5194/egusphere-2025-365
Preprint. Discussion started: 10 February 2025

means 30%). j indicates the feature importance for each site. Note that the absolute IG values are normalized by using minimum and maximum IG values in each site. Thus, the values here with 1 most important, while 0 least important to the evaporative fraction predictions. Note that only sites with more than 10 years observations are summarized here.

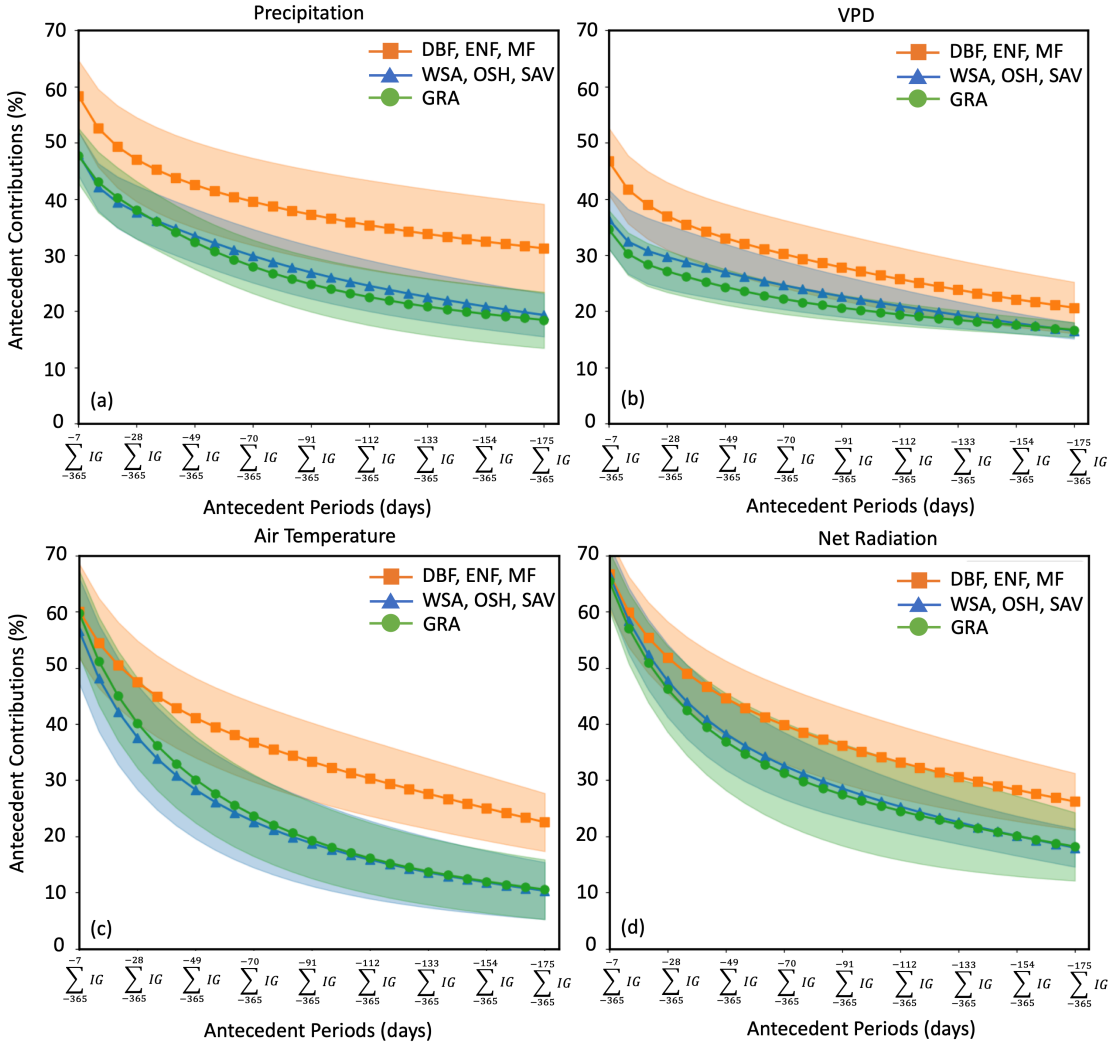

Figure 5. Memory Effect Contributions of Key Drivers in Predicting Evaporative Fraction. The sum of integrated gradients (IG) for different antecedent periods, e.g., $\sum_{-365}^{-7} \boldsymbol{IG}$ represents the sum of absolute IGs between previous 7 and 365 days, for precipitation (a), VPD (b), air temperature (c), net radiation (d). The sum absolute IGs are further normalized to a relative percent contribution for easy comparison. Note that only sites with more than 10 years of observations are summarized here, same with Figure 4.

Our temporal EF model, unlike non-temporal models in previous studies, distinguishes general feature influenced at individual time steps through integrated gradient values, shedding light on the temporal mechanics of EF. We then further summarize the IGs by different time steps, e.g., $\sum_{-365}^{-7} IG$ represents the sum of absolute IGs ranging from the previous 7 to 365 days, for different drivers (Methods). The sum absolute IGs are further normalized to a relative percent contribution for

https://doi.org/10.5194/egusphere-2025-365
Preprint. Discussion started: 10 February 2025

easy comparison. The memory effect here is indicated by the relative contributions (in %) of the antecedent time steps in each variable. We found varying memory effect across different PFTs, with relatively lower antecedent contributions for GRA, WSA than DBF, ENF and MF. For instance, 58% of the precipitation contribution to EF predictions for DBF, ENF and MF comes from antecedent precipitation $\sum_{-365}^{-7} IG$, followed by the 48% for WSA, OSH, SAV and GRA (Figure 5). For the forest sites, even precipitation from almost 6 months ago contributed 31% ($\sum_{-365}^{-175} IG$) to EF predictions (Figure 5). The maximum duration of the precipitation reveals that the legacy effect of winter precipitation, occurring 365 days prior, continues to impact water use strategies, as shown by our analysis. This observation aligns with the previous studies and experimental findings. For instance, antecedent winter precipitation from one or two years prior has been shown to influence growth in the current period(Bose et al., 2024; Kannenberg et al., 2020; Marqués et al., 2022; Shen et al., 2016). The contributions of the memory effect can also be observed for other variables, such as VPD, air temperature and net radiation (Figure 5). This indicates the different rooting depths and plant water use strategies that regulate the time scales of droughts, which deserved to be further investigated. Therefore, we emphasize that ignoring the memory effect or legacy effect can introduce bias in detecting the main drivers and hinder a comprehensive understanding of key processes.

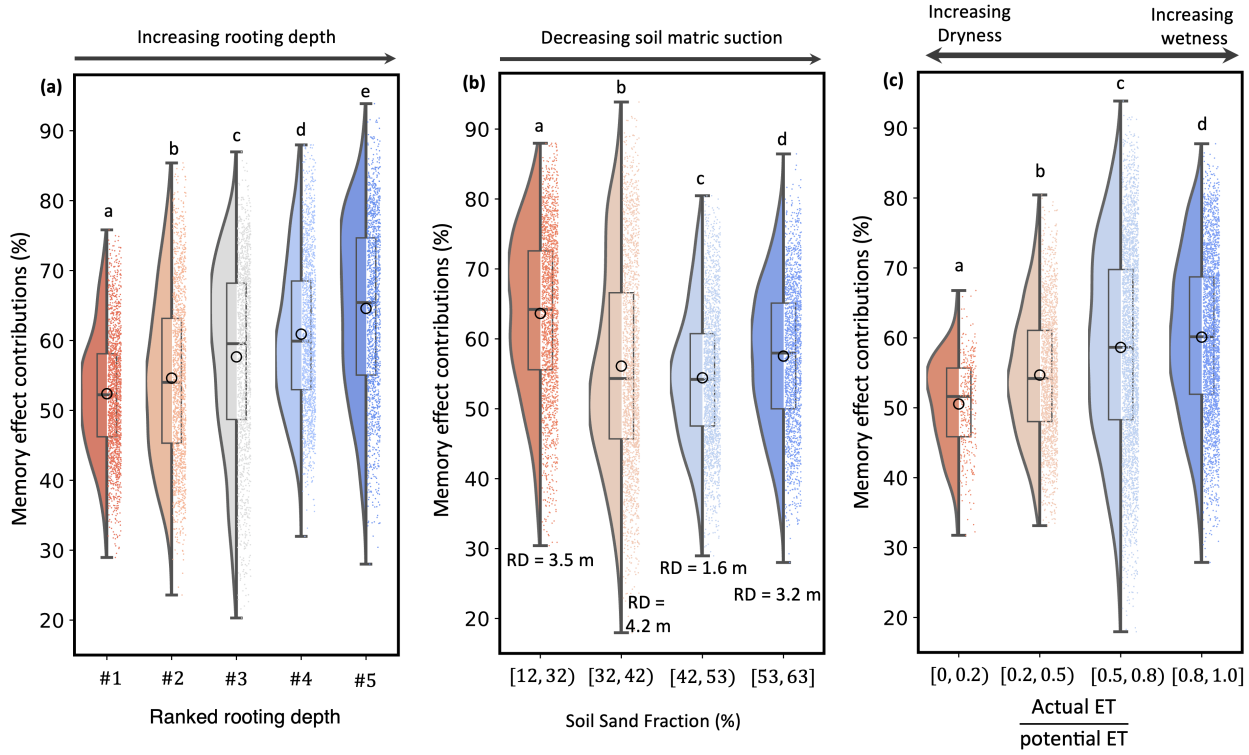

Figure 6. The Relationship Between Rooting Depth, Soil Water Holding Capacity, Aridity Index, and the Memory Effect as Captured by the Temporal Memory-Aware Model. The relationship between memory effect contributions to Evaporative Fraction predictions and the rooting depth (a), soil sand fraction (b), annual mean ratio of actual to potential evapotranspiration (c). Memory effect is defined as the sum of integrated gradients (IG) for antecedent periods, this is, $\sum_{-365}^{-7} \boldsymbol{IG}$ represents the sum of absolute IGs between previous 7 and 365 days, for precipitation. The sum absolute IGs are further normalized to a relative percent contribution compared to the concurrent effect ($\sum_{-7}^{0} \boldsymbol{IG}$) for each EF predictions. Note that only sites with more than 10 years of observations are summarized here,

https://doi.org/10.5194/egusphere-2025-365
Preprint. Discussion started: 10 February 2025

same with Figure 4. In the box plots, the central lines represent the median values, the circle represent the mean values, the upper and lower box limits represent the 75th and 25th percentiles, and the upper and lower whiskers extend to 1.5 times the interquartile range, respectively. The violin plot shows the data points density distributions. Letters denote statistically significant differences in the average memory effect contributions values (Tukey's HSD test, $P<0.05$). The annual mean ratio of actual to potential evapotranspiration is used as an aridity index, with values near 1 indicating wetter conditions and values 0 indicating drier conditions. Higher soil sand fractions correspond to lower soil matric suction. Deeper rooting depth enable plants to access more water stored from the previous wet season (as illustrated in Figure 1(a)). Data sources include TerraClimate (for the annual mean actual evapotranspiration and potential evapotranspiration) via Google Earth Engine (Abatzoglou et al., 2018), soil sand fraction data from SoilGrid (Poggio et al., 2021) and rooting depth data from Stocker et al., 2023.

We further explored the hidden information within the memory effect by examining its relationship with soil sand fraction (an indicator of soil matric suction and soil water holding capacity), rooting depth, and the annual mean ratio of actual to potential evapotranspiration (an aridity index representing dryness and wetness) across different PFTs. The results underscore the importance of the memory effect captured by our model in reflecting diverse plant water use strategies, as initially motivated in Figure 1 to use fast and slow EF decay rates to infer plant water use strategies. Our findings reveal that the memory effect increases with deeper plant rooting depths. Vegetation with deep roots, such as forests, can access deep soil water storage derived from precipitation during antecedent periods, resulting in a stronger memory effect (averaging up to 65% contribution). Conversely, vegetation with shallow roots relies more on soil water stored in recent periods, showing a weaker memory effect (52% contribution on average). These results highlight the potential of EF dynamics to serve as indicators of plant water stress and water use strategies. Additionally, plant-available water storage is influenced not only by rooting depth but also by soil water holding capacity(Piedallu et al., 2011). When we examined the relationship between memory effect and soil sand fraction, we found that higher soil sand fractions corresponding to a decreasing memory effect due to reduced soil suction, which limits the soil's ability to retain precipitation from antecedent periods. In the field experiments, sandy soil was found to hold significantly less plant-available water per foot of soil compared to silt loam (Shwetha and Varija, 2015; Verheijen et al., 2019). While there is a general monotonic decrease in the memory effect with increasing soil sand fraction, rooting depth remains a critical factor, with both factors jointly regulating plant water use strategies (Figure 6(b)).

These findings further explain the monotonic increase in memory effect with the aridity index observed in Figure 6(c). In dry areas, such as woody savannas, savannas, and open shrublands, shallow rooting depths and high soil sand fractions (e.g., in deserts or the Gobi region) result in lower memory effect contributions (51% on average for aridity indices between 0 and 0.2). In wetter areas, forests with deeper rooting depths and lower soil sand fractions are better equipped to utilize water stored from antecedent precipitation, resulting in higher memory effects (60% on average for aridity indices between 0.8 and 1.0). Our analysis suggests that the memory effect holds potential as a proxy for rooting depth - a factor that are often difficult to measure and have been largely overlooked in many studies and Earth system models. However, further investigation is still required to fully understand to the complex mechanisms governing the interaction between these factors. Neglecting the memory effect could lead to a reduced understanding of the water, energy and carbon cycle, limiting our ability to model and predict these critical processes accurately.

https://doi.org/10.5194/egusphere-2025-365
Preprint. Discussion started: 10 February 2025

5 Conclusions

In this study, using eddy-covariance data from the combined ICOS, AmeriFlux, Fluxnet2015 Tier 1 dataset, we developed a memory-aware machine learning model that integrates the memory effect of weather data to predict Evaporative Fraction, which is a key indicator of plant water stress conditions. Our findings reveal:

1) The model delivers robust performance across various plant functional types for sites not encountered during training.
2) The model adequately captures and reconstructs the EF dynamics, particularly during soil moisture dry-down periods very well and these observations are consistent with soil moisture decay patterns.
3) By accounting for the memory effect, air temperature and precipitation rather than net radiation, emerged as the most influential driver of EF predictions, followed by VPD. Notably, the integrated gradients' temporal analysis indicated that the model accounts for more historical time steps for forest sites compared to woody savanna and grassland sites, likely due to differences in vegetation rooting depths and water usage strategies. Our analysis suggests that the typical maximum duration for forest sites extends to one year, whereas woody savanna and grassland sites generally rely on shorter time periods, spanning several months, for most of EF predictions.
4) Further investigation reveals that memory effect is closely associated with rooting depth, soil sandy fractions, and aridity index. These findings highlight novel mechanisms that emerge only when the memory effect is considered. This underscores the potential of using the EF across diverse PFTs to reflect varying plant water stress conditions and water use strategies.

Our results highlight the critical importance of the memory effect in EF predictions and carry significant implications for assessing ecosystem water stress and predicting it months in advance. For instance, water shortages from the previous year can still impact ecosystem functioning in the current year, particularly in forests. Incorporating this memory-awareness into our modeling approach opens new opportunities to infer varying rooting depth across biomes from surface measurements – an important yet often overlooked factor in land surface and earth system modeling.

Acknowledgments

P.G. and W.Z. would like to acknowledge funding from the Land Ecosystem Models based On New Theory, obseRvations and ExperimEnts (LEMONTREE) project, and National Science Foundation Science and Technology Center LEAP, Learning the Earth with Artificial intelligence and Physics, as well as support from NASA grant 80NSSC18K0998. A.J.W., P.G. and W.Z., M.R. acknowledge support by the European Research Council (ERC) Synergy Grant "Understanding and Modelling the Earth System with Machine Learning (USMILE)" under the Horizon 2020 research and innovation program (Grant agreement No.855187). W.Z. would like to acknowledge the scholarship awarded by the Max Planck Institute for Biogeochemistry. We extend our sincere thanks to Dr. Christian Reimers from the Max Planck Institute for Biogeochemistry for reviewing and improving the readability of the entire manuscript.

https://doi.org/10.5194/egusphere-2025-365
Preprint. Discussion started: 10 February 2025

Author contributions

W. Z., A.J. W., and P. G. designed the study. W.Z. performed the analyses, with additional support from Ulrich Weber on datasets preprocessing. W.Z. led the writing with input from all co-authors.

Competing financial interests

Some authors are members of the editorial board of journal Hydrology and Earth System Sciences.

References

Abatzoglou, J. T., Dobrowski, S. Z., Parks, S. A., and Hegewisch, K. C.: TerraClimate, a high-resolution global dataset of monthly climate and climatic water balance from 1958–2015, Sci Data, 5, 170191, https://doi.org/10.1038/sdata.2017.191, 2018.

Bastiaanssen, W. G. M., Pelgrum, H., Droogers, P., De Bruin, H. A. R., and Menenti, M.: Area-average estimates of evaporation, wetness indicators and top soil moisture during two golden days in EFEDA, Agricultural and Forest Meteorology, 87, 119–137, https://doi.org/10.1016/S0168-1923(97)00020-8, 1997.

Bose, A. K., Doležal, J., Scherrer, D., Altman, J., Ziche, D., Martínez-Sancho, E., Bigler, C., Bolte, A., Colangelo, M., Dorado-Liñán, I., Drobyshev, I., Etzold, S., Fonti, P., Gessler, A., Kolář, T., Koňasová, E., Korznikov, K. A., Lebourgeois, F., Lucas-Borja, M. E., Menzel, A., Neuwirth, B., Nicolas, M., Omelko, A. M., Pederson, N., Petritan, A. M., Rigling, A., Rybníček, M., Scharnweber, T., Schröder, J., Silla, F., Sochová, I., Sohar, K., Ukhvatkina, O. N., Vozmishcheva, A. S., Zweifel, R., and Camarero, J. J.: Revealing legacy effects of extreme droughts on tree growth of oaks across the Northern Hemisphere, Science of The Total Environment, 926, 172049, https://doi.org/10.1016/j.scitotenv.2024.172049, 2024.

Chen, Y., Xue, Y., and Hu, Y.: How multiple factors control evapotranspiration in North America evergreen needleleaf forests, Science of The Total Environment, 622–623, 1217–1224, https://doi.org/10.1016/j.scitotenv.2017.12.038, 2018.

Collins, D. B. G. and Bras, R. L.: Plant rooting strategies in water-limited ecosystems, Water Resources Research, 43, 2006WR005541, https://doi.org/10.1029/2006WR005541, 2007.

Dirmeyer, P. A., Zeng, F. J., Ducharne, A., Morrill, J. C., and Koster, R. D.: The Sensitivity of Surface Fluxes to Soil Water Content in Three Land Surface Schemes, J. Hydrometeor, 1, 121–134, https://doi.org/10.1175/1525-7541(2000)001<0121:TSOSFT>2.0.CO;2, 2000.

Dong, J., Akbar, R., Short Gianotti, D. J., Feldman, A. F., Crow, W. T., and Entekhabi, D.: Can Surface Soil Moisture Information Identify Evapotranspiration Regime Transitions?, Geophysical Research Letters, 49, e2021GL097697, https://doi.org/10.1029/2021GL097697, 2022.

Dralle, D. N., Jesse Hahm, W., Rempe, D. M., Karst, N., Anderegg, L. D. L., Thompson, S. E., Dawson, T. E., and Dietrich, W. E.: Plants as sensors: vegetation response to rainfall predicts root-zone water storage capacity in Mediterranean-type climates, Environ. Res. Lett., 15, 104074, https://doi.org/10.1088/1748-9326/abb10b, 2020.

https://doi.org/10.5194/egusphere-2025-365
Preprint. Discussion started: 10 February 2025

ElGhawi, R., Kraft, B., Reimers, C., Reichstein, M., Körner, M., Gentine, P., and Winkler, A. J.: Hybrid modeling of evapotranspiration: inferring stomatal and aerodynamic resistances using combined physics-based and machine learning, Environ. Res. Lett., 18, 034039, https://doi.org/10.1088/1748-9326/acbbe0, 2023.

Fan, Y., Miguez-Macho, G., Jobbágy, E. G., Jackson, R. B., and Otero-Casal, C.: Hydrologic regulation of plant rooting depth, Proc. Natl. Acad. Sci. U.S.A., 114, 10572–10577, https://doi.org/10.1073/pnas.1712381114, 2017.

Fang, K. and Shen, C.: Near-real-time forecast of satellite-based soil moisture using long short-term memory with an adaptive data integration kernel, Journal of Hydrometeorology, 21, 399–413, 2020.

Feng, D., Fang, K., and Shen, C.: Enhancing Streamflow Forecast and Extracting Insights Using Long-Short Term Memory Networks With Data Integration at Continental Scales, Water Resources Research, 56, e2019WR026793, https://doi.org/10.1029/2019WR026793, 2020.

Foken, T.: The energy balance closure problem: An overview, Ecological Applications, 18, 1351–1367, 2008.

Fu, Z., Ciais, P., Makowski, D., Bastos, A., Stoy, P. C., Ibrom, A., Knohl, A., Migliavacca, M., Cuntz, M., Šigut, L., Peichl, M., Loustau, D., El-Madany, T. S., Buchmann, N., Gharun, M., Janssens, I., Markwitz, C., Grünwald, T., Rebmann, C., Mölder, M., Varlagin, A., Mammarella, I., Kolari, P., Bernhofer, C., Heliasz, M., Vincke, C., Pitacco, A., Cremonese, E., Foltýnová, L., and Wigneron, J.: Uncovering the critical soil moisture thresholds of plant water stress for European ecosystems, Global Change Biology, 28, 2111–2123, https://doi.org/10.1111/gcb.16050, 2022.

Gentine, P., Entekhabi, D., Chehbouni, A., Boulet, G., and Duchemin, B.: Analysis of evaporative fraction diurnal behaviour, Agricultural and Forest Meteorology, 143, 13–29, https://doi.org/10.1016/j.agrformet.2006.11.002, 2007.

Gentine, P., Entekhabi, D., and Polcher, J.: The Diurnal Behavior of Evaporative Fraction in the Soil–Vegetation–Atmospheric Boundary Layer Continuum, Journal of Hydrometeorology, 12, 1530–1546, https://doi.org/10.1175/2011JHM1261.1, 2011.

Guérin, M., Von Arx, G., Martin-Benito, D., Andreu-Hayles, L., Griffin, K. L., McDowell, N. G., Pockman, W., and Gentine, P.: Distinct xylem responses to acute vs prolonged drought in pine trees, Tree Physiology, 40, 605–620, https://doi.org/10.1093/treephys/tpz144, 2020.

Haghighi, E., Short Gianotti, D. J., Akbar, R., Salvucci, G. D., and Entekhabi, D.: Soil and Atmospheric Controls on the Land Surface Energy Balance: A Generalized Framework for Distinguishing Moisture-Limited and Energy-Limited Evaporation Regimes, Water Resources Research, 54, 1831–1851, https://doi.org/10.1002/2017WR021729, 2018.

Hollinger, D. and Richardson, A.: Uncertainty in eddy covariance measurements and its application to physiological models, Tree physiology, 25, 873–885, 2005.

Ichii, K., Wang, W., Hashimoto, H., Yang, F., Votava, P., Michaelis, A. R., and Nemani, R. R.: Refinement of rooting depths using satellite-based evapotranspiration seasonality for ecosystem modeling in California, Agricultural and Forest Meteorology, 149, 1907–1918, https://doi.org/10.1016/j.agrformet.2009.06.019, 2009.

Jiang, S., Zheng, Y., and Solomatine, D.: Improving AI System Awareness of Geoscience Knowledge: Symbiotic Integration of Physical Approaches and Deep Learning, Geophys Res Lett, 47, https://doi.org/10.1029/2020GL088229, 2020.

Jiang, S., Bevacqua, E., and Zscheischler, J.: River flooding mechanisms and their changes in Europe revealed by explainable machine learning, Hydrol Earth Syst Sc, 26, 6339–6359, https://doi.org/10.5194/hess-26-6339-2022, 2022.

https://doi.org/10.5194/egusphere-2025-365
Preprint. Discussion started: 10 February 2025

Kannenberg, S. A., Schwalm, C. R., and Anderegg, W. R. L.: Ghosts of the past: how drought legacy effects shape forest functioning and carbon cycling, Ecology Letters, 23, 891–901, https://doi.org/10.1111/ele.13485, 2020.

Kraft, B., Jung, M., Körner, M., Requena Mesa, C., Cortés, J., and Reichstein, M.: Identifying Dynamic Memory Effects on Vegetation State Using Recurrent Neural Networks, Front. Big Data, 2, 31, https://doi.org/10.3389/fdata.2019.00031, 2019.

Kraft, B., Jung, M., Körner, M., Koirala, S., and Reichstein, M.: Towards hybrid modeling of the global hydrological cycle, Hydrol. Earth Syst. Sci., 26, 1579–1614, https://doi.org/10.5194/hess-26-1579-2022, 2022.

Lees, T., Reece, S., Kratzert, F., Klotz, D., Gauch, M., De Bruijn, J., Kumar Sahu, R., Greve, P., Slater, L., and Dadson, S.: Hydrological concept formation inside long short-term memory (LSTM) networks, Hydrology and Earth System Sciences Discussions, 2021, 1–37, 2021.

Lees, T., Reece, S., Kratzert, F., Klotz, D., Gauch, M., De Bruijn, J., Kumar Sahu, R., Greve, P., Slater, L., and Dadson, S. J.: Hydrological concept formation inside long short-term memory (LSTM) networks, Hydrol. Earth Syst. Sci., 26, 3079–3101, https://doi.org/10.5194/hess-26-3079-2022, 2022.

Lhomme, J.-P. and Elguero, E.: Examination of evaporative fraction diurnal behaviour using a soil-vegetation model coupled with a mixed-layer model, Hydrology and Earth System Sciences, 3, 259–270, 1999.

Li, Q., Zhu, Y., Shangguan, W., Wang, X., Li, L., and Yu, F.: An attention-aware LSTM model for soil moisture and soil temperature prediction, Geoderma, 409, 115651, https://doi.org/10.1016/j.geoderma.2021.115651, 2022.

Lian, X., Zhao, W., and Gentine, P.: Recent global decline in rainfall interception loss due to altered rainfall regimes, Nat Commun, 13, 7642, https://doi.org/10.1038/s41467-022-35414-y, 2022.

Liu, X., Chen, F., Barlage, M., and Niyogi, D.: Implementing Dynamic Rooting Depth for Improved Simulation of Soil Moisture and Land Surface Feedbacks in Noah-MP-Crop, J Adv Model Earth Sy, 12, https://doi.org/10.1029/2019MS001786, 2020.

Loveland, T. R., Reed, B. C., Brown, J. F., Ohlen, D. O., Zhu, Z., Yang, L., and Merchant, J. W.: Development of a global land cover characteristics database and IGBP DISCover from 1 km AVHRR data, International journal of remote sensing, 21, 1303–1330, 2000.

Lu, Y., Dong, J., Steele-Dunne, S. C., and Van De Giesen, N.: Estimating surface turbulent heat fluxes from land surface temperature and soil moisture observations using the particle batch smoother, Water Resources Research, 52, 9086–9108, https://doi.org/10.1002/2016WR018943, 2016.

Marqués, L., Peltier, D. M. P., Camarero, J. J., Zavala, M. A., Madrigal-González, J., Sangüesa-Barreda, G., and Ogle, K.: Disentangling the Legacies of Climate and Management on Tree Growth, Ecosystems, 25, 215–235, https://doi.org/10.1007/s10021-021-00650-8, 2022.

Molnar, C.: Interpretable machine learning, 2019.

Nutini, F., Boschetti, M., Candiani, G., Bocchi, S., and Brivio, P.: Evaporative Fraction as an Indicator of Moisture Condition and Water Stress Status in Semi-Arid Rangeland Ecosystems, Remote Sensing, 6, 6300–6323, https://doi.org/10.3390/rs6076300, 2014.

O., S. and Orth, R.: Global soil moisture data derived through machine learning trained with in-situ measurements, Sci Data, 8, 170, https://doi.org/10.1038/s41597-021-00964-1, 2021.

https://doi.org/10.5194/egusphere-2025-365
Preprint. Discussion started: 10 February 2025

Pan, S., Pan, N., Tian, H., Friedlingstein, P., Sitch, S., Shi, H., Arora, V. K., Haverd, V., Jain, A. K., and Kato, E.: Evaluation of global terrestrial evapotranspiration using state-of-the-art approaches in remote sensing, machine learning and land surface modeling, Hydrology and Earth System Sciences, 24, 1485–1509, 2020.

Piedallu, C., Gégout, J.-C., Bruand, A., and Seynave, I.: Mapping soil water holding capacity over large areas to predict potential production of forest stands, Geoderma, 160, 355–366, https://doi.org/10.1016/j.geoderma.2010.10.004, 2011.

Poggio, L., de Sousa, L. M., Batjes, N. H., Heuvelink, G. B. M., Kempen, B., Ribeiro, E., and Rossiter, D.: SoilGrids 2.0: producing soil information for the globe with quantified spatial uncertainty, SOIL, 7, 217–240, https://doi.org/10.5194/soil-7-217-2021, 2021.

Reichstein, M., Camps-Valls, G., Stevens, B., Jung, M., Denzler, J., Carvalhais, N., and Prabhat, fnm: Deep learning and process understanding for data-driven Earth system science, Nature, 566, 195–204, 2019.

Reichstein, M., Ahrens, B., Kraft, B., Camps-Valls, G., Carvalhais, N., Gans, F., Gentine, P., and Winkler, A. J.: Combining system modeling and machine learning into hybrid ecosystem modeling, in: Knowledge Guided Machine Learning, Chapman and Hall/CRC, 327–352, 2022.

Richardson, A. D., Hollinger, D. Y., Burba, G. G., Davis, K. J., Flanagan, L. B., Katul, G. G., Munger, J. W., Ricciuto, D. M., Stoy, P. C., and Suyker, A. E.: A multi-site analysis of random error in tower-based measurements of carbon and energy fluxes, Agricultural and Forest Meteorology, 136, 1–18, 2006.

Schwalm, C. R., Williams, C. A., Schaefer, K., Arneth, A., Bonal, D., Buchmann, N., Chen, J., Law, B. E., Lindroth, A., Luyssaert, S., Reichstein, M., and Richardson, A. D.: Assimilation exceeds respiration sensitivity to drought: A FLUXNET synthesis, Global Change Biology, 16, 657–670, https://doi.org/10.1111/j.1365-2486.2009.01991.x, 2010.

Seyfried, M. S. and Wilcox, B. P.: Soil water storage and rooting depth: key factors controlling recharge on rangelands, Hydrological Processes, 20, 3261–3275, https://doi.org/10.1002/hyp.6331, 2006.

Shen, W., Jenerette, G. D., Hui, D., and Scott, R. L.: Precipitation legacy effects on dryland ecosystem carbon fluxes: direction, magnitude and biogeochemical carryovers, Biogeosciences, 13, 425–439, https://doi.org/10.5194/bg-13-425-2016, 2016.

Shwetha, P. and Varija, K.: Soil Water Retention Curve from Saturated Hydraulic Conductivity for Sandy Loam and Loamy Sand Textured Soils, Aquatic Procedia, 4, 1142–1149, https://doi.org/10.1016/j.aqpro.2015.02.145, 2015.

Skulovich, O. and Gentine, P.: A Long-term Consistent Artificial Intelligence and Remote Sensing-based Soil Moisture Dataset, Sci Data, 10, 154, https://doi.org/10.1038/s41597-023-02053-x, 2023.

Stocker, B. D., Tumber-Dávila, S. J., Konings, A. G., Anderson, M. C., Hain, C., and Jackson, R. B.: Global patterns of water storage in the rooting zones of vegetation, Nat. Geosci., https://doi.org/10.1038/s41561-023-01125-2, 2023.

Sundararajan, M., Taly, A., and Yan, Q.: Axiomatic Attribution for Deep Networks, http://arxiv.org/abs/1703.01365, 12 June 2017.

Verheijen, F. G. A., Zhuravel, A., Silva, F. C., Amaro, A., Ben-Hur, M., and Keizer, J. J.: The influence of biochar particle size and concentration on bulk density and maximum water holding capacity of sandy vs sandy loam soil in a column experiment, Geoderma, 347, 194–202, https://doi.org/10.1016/j.geoderma.2019.03.044, 2019.

https://doi.org/10.5194/egusphere-2025-365
Preprint. Discussion started: 10 February 2025

Wang, K., Li, Z., and Cribb, M.: Estimation of evaporative fraction from a combination of day and night land surface temperatures and NDVI: A new method to determine the Priestley–Taylor parameter, Remote Sensing of Environment, 102, 293–305, https://doi.org/10.1016/j.rse.2006.02.007, 2006.

Williams, I. N. and Torn, M. S.: Vegetation controls on surface heat flux partitioning, and land-atmosphere coupling, Geophysical Research Letters, 42, 9416–9424, https://doi.org/10.1002/2015GL066305, 2015.

Yang, W., Shabanov, N., Huang, D., Wang, W., Dickinson, R., Nemani, R., Knyazikhin, Y., and Myneni, R.: Analysis of leaf area index products from combination of MODIS Terra and Aqua data, Remote Sensing of Environment, 104, 297–312, 2006.

Zenone, T., Vitale, L., Famulari, D., and Magliulo, V.: Application of machine learning techniques to simulate the evaporative fraction and its relationship with environmental variables in corn crops, Ecol Process, 11, 54, https://doi.org/10.1186/s13717-022-00400-1, 2022.

Zhao, W. L., Gentine, P., Reichstein, M., Zhang, Y., Zhou, S., Wen, Y., Lin, C., Li, X., and Qiu, G. Y.: Physics-Constrained Machine Learning of Evapotranspiration, Geophysical Research Letters, 46, 14496–14507, https://doi.org/10.1029/2019GL085291, 2019.